Optics & Laser Technology 147 (2022) 107629

Contents lists available at ScienceDirect

Optics and Laser Technology

journal homepage: www.elsevier.com/locate/optlastec

Lock-in thermography using miniature infra-red cameras and integrated actuators for defect identification in composite materials

G. Ólafsson [a,c,*], R.C. Tighe [b], S.W. Boyd [a], J.M. Dulieu-Barton [c]

[a] School of Engineering, Boldrewood Innovation Campus, University of Southampton, Southampton, UK
[b] School of Engineering, University of Waikato, Hamilton, New Zealand
[c] Bristol Composites Institute, School of Civil, Aerospace and Mechanical Engineering, University of Bristol, Bristol, UK

ARTICLE INFO

Keywords:
Non-destructive evaluation (NDE)
Lock-in thermography (LIT)
Bolometer
Internal heating
Embedded actuator

ABSTRACT

A novel approach for thermographic Non-Destructive Evaluation (NDE) of laminated polymer composite structures is presented. The technique is based on Lock-In Thermography (LIT), which traditionally uses an external heat source. Here a new means of internal heating, via a lightweight embedded actuator capable of providing highly repeatable and uniform heating is presented. The equipment cost, complexity and hence size is reduced by removing the need for high power external thermal excitation. Instead, the necessary temperature modulation of the internal actuator is achieved with a compact and low-cost Arduino controlled circuit. The size and cost of the equipment is further reduced by demonstrating that a miniature printed circuit board mounted thermal core type micro-bolometer can be used effectively for LIT. The performance of the thermal core is quantitatively compared with the more expensive and bulky traditional infra-red cameras. It is shown that the thermal core can detect defects with similar overall performance as a cooled photon detector and an uncooled micro-bolometer. The low-cost, compact nature and small mass of the thermal core offers great potential in thermographic inspection opening the possibility of deploying devices permanently on structures in conjunction with the embedded actuators for in-situ monitoring in the service environment.

1. Introduction

Defects can occur in fibre reinforced polymer composite materials either during manufacturing, or in-service, which can significantly reduce component strength and stiffness [1]. Accurate and expedient identification of defects is therefore crucial, especially in safety critical applications [2]. Thermography offers advantages over other inspection techniques as it is rapid, non-contact and can provide quantitative full field data [3]. Lock-in Thermography (LIT) [4,5], or modulated thermography, is a type of active thermography, which uses an external modulated energy source, usually in the form of high power lamps, to heat the component surface and provide the necessary heating for defect detection. Thermal waves propagate into the component at the modulation frequency and are reflected at interfaces where there is a change in thermal properties, e.g. at the component back surface, or at a defect. The reflected waves propagate back to the front surface, where an infra-red (IR) camera monitors the surface thermal response. The acquired thermal data is then processed using digital lock-in data processing, which applies notch filtering at the frequency of the thermal modulation. Hence the thermal response to the input sinusoidal thermal excitation is isolated from other response features [6]. This is achieved by correlating the acquired thermal signals measured by each pixel in an IR camera with the excitation signal to obtain the amplitude and phase of the response. A comparative assessment of either amplitude or phase can be made across a field of view where the response at defective and non-defective regions differ, thus allowing a defect to be identified and its shape characterised.

The probing depth of thermographic inspections of polymer composites are limited by the low thermal diffusivity [7], which restricts its application to relatively thin laminates. As composites are used increasingly for primary structures e.g. aircraft [8], the thickness of typical laminates in many applications must increase and hence probing depth is increasingly a key limitation of thermography for inspection. Of the available techniques, LIT has been shown achieve greater probing depths than other thermographic inspection methods [9]. While probing depth is ultimately limited by the thermal diffusion length of a thermal wave, the thermal or phase contrast, which enables defect detection, is typically increased with additional thermal energy input. LIT also has

* Corresponding author.
E-mail address: geir.olafsson@bristol.ac.uk (G. Ólafsson).

https://doi.org/10.1016/j.optlastec.2021.107629
Received 3 June 2021; Received in revised form 10 September 2021; Accepted 1 November 2021
Available online 19 November 2021

advantages over techniques such as Pulsed Thermography (PT) [10], a technique in which a short duration heat pulse provides thermal excitation and the pulse energy must be increased to probe deeper through the thickness of a component. In the case of composite materials, increasing the pulse excitation energy to excess will result in high surface temperatures, potentially causing damage. LIT does not require a pulse and instead uses a sinusoidally varying thermal stimulus applied over set durations. Concentrating energy to a single frequency allows additional thermal energy input. In addition, the inspection duration can easily be increased to impart greater thermal energy into a component. The combination of these two advantages enable high contrast results whilst minimising the likelihood of inflicting thermal damage during inspections [11].

Whilst thermography is established in certain industries as a common NDT technique [3], a limitation of LIT is that the heating lamps can be cumbersome and require clear lines of sight to the inspected component. This limits the application of LIT to areas of a structure with good access where bulky cameras and lamps can be suitably accommodated. Typical inspection systems also rely on special purpose modulation units for sinusoidal thermal excitation modulation. In the present paper, new unobtrusive embedded heating elements, i.e. actuators, are incorporated within the structure to significantly reduce the access area required to carry out inspections. Moreover, placing heating elements within a component allows for a reduction in the effective component thickness assuming that two sided inspections are possible. This has the benefit of increasing the probing depth of LIT as the thermal wave propagation is a function of material thickness. Furthermore, a versatile, compact and low-cost circuit configuration is proposed capable of modulating the heating of the proposed embedded actuator yet could also be used to modulate any direct current heating device.

Traditionally, LIT has been carried out using photon detector-based IR cameras, which are cryogenically cooled using an inbuilt sterling cooling system. Hence, the cameras are very costly (~100 k USD), fragile and bulky, all of which act as a barrier to deployment in the service environment. Uncooled micro-bolometer IR cameras provide a potential alternative device for LIT as they are a factor of 10 less expensive than the photon detectors, are more lightweight and rugged. These advantages have motivated recent studies into the use of research grade micro-bolometers in thermographic inspection applications e.g. [12–14]. An inconvenience of many micro-bolometer based cameras, compared to those based on photon detectors, is that they do not have an in-built facility to simultaneously record an external signal with the IR image capture. This means a reference signal cannot be supplied directly into the camera, which is time-stamped with the thermal images to facilitates straightforward application of the lock-in procedure. In addition, the typical sensitivity and responsiveness of micro-bolometers is inherently lower than photon detectors. Despite these limitations, the recently introduced miniature thermal core printed circuit board mounted micro-bolometer based cameras [15], costing as little as 300 USD, has prompted the present investigation into their applicability for LIT. The small format and low cost of the thermal core, in combination with the embedded actuators proposed in the paper, offer a new methodology for LIT with the potential for permanent deployment on a structure and a route to thermography based structural health monitoring.

The efficacy of the proposed new LIT methodology is confirmed by demonstrating that:

1. An existing embedded feature can be used to provide sufficient excitation to permit LIT.
2. A new compact and low-cost modulation circuit using open source components and software can be used to generate the excitation in the existing embedded feature.
3. A low-cost miniature thermal core camera has sufficient sensitivity to perform LIT and thus reduce the overall cost of thermographic inspections by more than two orders of magnitude.

The paper starts with an overview of the image processing routine used for LIT; several options are available, so a justification is provided for the approach adopted. Next, a description is provided of the three types of IR camera used to obtain the thermal response: a Telops Fast MK2 photon detector, a FLIR AC655 micro-bolometer and a FLIR Lepton 3.5 thermal core bolometer. The detectors used in each camera have decreasing sensitivity and accuracy respectively, however this is also accompanied by an order of magnitude cost reduction. A description of the design of the modulation circuit and connection to embedded actuator is provided. It is explained how a commercially available compact Arduino, can be combined with other components to provide the modulation. It is envisaged that the internal actuation could be facilitated by using existing conductive features, such as electromagnetic screening, lightning protection etc. However, the methodology is not limited to components that require these internal conductive features. The feature used in this work as is commerically used for electromagnetic screeing. The material is lightweight (34 gsm) and electrically conductive has been shown not cause any discernible structural knockdown when incorporated between plies in a composite laminate or within a bond line of a bonded joint [16]. The LIT methodology is demonstrated on component comprising a glass fibre reinforced epoxy composite specimen, with an embedded feature that mimics electromagnetic screening using the same material as [16]. The results from the demonstration component show that a range of simulated defects, with different sizes and depths, can be detected effectively by all three IR cameras used in the proposed LIT methodology. Hence a new compact, unobtrusive, robust and low-cost solution for IR inspections of composite structures is proposed.

2. Thermal image processing

2.1. Lock-in processing

The application of a sinusoidal heat source to the specimen under inspection is a fundamental part of LIT, as this facilitates the use of lock-in processing which acts as a notch filter and allows the phase and magnitude of the thermal response to be easily obtained. Either magnitude or phase can be used to detect defects, whereby the response in defective regions differs from non-defective regions. Busse [9] showed that the phase images performed better than magnitude because the magnitude of the response is affected by heating non-uniformities adding systematic error to the resulting magnitude data, whereas the phase of response is unaffected by this effect.

While the early implementations of LIT required use of the lock-in amplifiers, the modern-day digitisation of thermal data has facilitated a multitude of computational approaches. A common approach is to transform the thermal temporal data into the frequency domain using a Fourier transform to extract the phase of the response at the modulation frequency [4]. Others [17] have suggested the use of wavelet transforms, which has the advantage of retaining temporal information post processing. An alternative approach suggested in [13] performs a least squared regression to obtain the phase and amplitude of the thermal response. This conveniently harnesses the powerful and computationally efficient matrix manipulation capabilities of software such as Matlab. Whilst it is acknowledged that these approaches may improve processing efficiency or enhance output data, to facilitate comparison to a wider body of research a traditional processing approach based on the digital lock-in amplifier was implemented in this work.

LIT is reliant on the appropriate selection of modulation frequency, since thermal waves are highly attenuated, particularly in composites. Generally, the highest possible modulation frequency is preferable since thermal wave frequency is proportional to the achievable spatial resolution and hence ability to reliably identify small or irregular defects. However, low frequency waves propagate further, thus the modulation frequency must be reduced with increasing component thickness. This is a well-known limitation of LIT which has even prompted development

of new techniques to overcome the need for this compromise, e.g. chirped excitation with matched filtering [18], although not widely adopted. Hence, the traditional sinusoidal modulation is applied in the current work.

The principle of LIT is to correlate the thermal response measured by each pixel of the IR camera, with a reference signal from the heating modulation unit. The thermal response is amplified at the frequency equal to the modulation frequency, improving the signal to noise ratio [19], and isolating the sinusoidal thermal response from background heat sources which are not generated sinusoidally or at the modulation frequency. The type of lock-in amplification used in LIT is phase sensitive, and therefore two lock-in amplifications are performed where the reference signal and its quadrature (X and Y respectively) are used; X is given by:

$$X = \frac{1}{N/2}\sum_{i=1}^{N} f(t_i)\sin(\omega t_i + \Phi) \tag{1}$$

where total number of frames in a recording and the frame number are given by N and i respectively. The input signal to the lock-in amplifier is represented by $f(t_i)$, as a function of time, t . The sinusoidal function represents the reference signal where ω and Φ denote frequency and phase respectively.

Y is given by:

$$Y = \frac{1}{N/2}\sum_{i=1}^{N} f(t_i)\cos(\omega t_i + \Phi) \tag{2}$$

where $\cos(\omega t_i + \Phi)$ is the quadrature of the reference signal.

Eqs. (2) and (3) are combined to obtain the amplitude of the response, A, as follows:

$$A = \sqrt{X^2 + Y^2} \tag{3}$$

with the phase, Φ, given by:

$$\Phi = tan^{-1}\left(\frac{Y}{X}\right) \tag{4}$$

2.2. Quantitative thermographic comparisons

A valuable feature of thermographic inspections is that full field image data are obtained, enabling a qualitative visual interpretation of the results, where defects are identified using the contrast between defective and non-defective regions. However, in comparing results from different inspections, and particularly when evaluating the effectiveness of one technique over another, a qualitative approach can be misleading. Specifically, the units associated with the data may differ between inspection approach (e.g. comparing phase and temperature data), and the scales at which the various data are visualised can make fair comparisons impossible. Vavilov [20] presented a convenient method of overcoming this issue by calculating the signal to noise ratio defined as

$$SNR = \frac{\overline{T_d} - \overline{T_{nd}}}{\sigma_{nd}} \tag{5}$$

where the mean across an area representing defective and non-defective regions $\overline{T_d}$ and $\overline{T_{nd}}$ respectively and σ_{nd} is the standard deviation across the non-defective region.

Eq. (5) provides a parameter describing both the magnitude of the contrast between the defective and non-defective regions, and the degree of random error present in the results data. The parameter enables a quantitative comparison between data of any type because it is non-dimensional and therefore signal to noise ratio is extensively used for the analysis and comparison of the data in the following sections of the paper. The signal to noise ratio was calculated using the phase and thermal magnitude images obtained from lock-in processing, whereby the defective regions were individually selected. Since the field of view in each case did not extend beyond the test specimen, all pixel data which was not identified as viewing a defective region was defined as non-defective. From these regions the mean temperatures of the non-defective and defective areas and the standard deviation of the non-defective area were calculated. Table 1 presents representative area sizes for each region considered, along side the standard deviation across the area from the temperature data.

2.3. IR cameras

Three IR cameras were used in this study, a photon detector (Telops MK2 Fast IR) and two micro-bolometers (FLIR AC655 and FLIR Lepton 3.5). Table 2 provides the performance characteristics and comparative costs of each camera. The photon detector is a cryogenically cooled Indium Antimonide (InSb) focal plane array (FPA) whereby a voltage is generated as a function of the number of photons impinging on each of the sensors in the array. The uncooled vanadium oxide (VOx) micro-bolometers have sensitivity and noise characteristics that are inferior to that of the photon detector. Furthermore, a micro-bolometer changes its electrical resistance in response to heat, introducing a time delay in its response, which acts as a low pass filter for transient signals such as those generated by LIT. For both camera types, the output voltage from the detector is fed into an Analogue to Digital Convertor (ADC) to obtain a digital signal that is then captured by the computer via a frame grabber and subsequently calibrated to a temperature measurement using calibration curves embedded into the computer software.

The key advantages of micro-bolometers stem from the use of uncooled sensors, significantly reducing the overall size and weight of the camera. Furthermore, the cost of research grade micro-bolometers (e.g. FLIR AC655) is significantly less than photon detectors. Recently printed circuit board mounted thermal core micro-bolometers have emerged on the market for approximately 300 USD, which is a fraction of the cost of even the traditional micro-bolometer cameras. The cost of the equipment has limited the use of thermography to large organisations and institutions which are willing and able to make substantial capital investments. While the performance of the printed circuit board mounted cameras is limited, the low cost significantly broadens the accessibility of thermography and represents an exciting opportunity to diversify thermographic applications. The key challenge remaining is to demonstrate that useful inspection data can be obtained, despite the limited performance of thermal core based micro-bolometers. The paper addresses this challenge and compares the achieved inspection performance against a traditional photon detector. A high grade AC655 micro-bolometer is included in the comparison to enable distinction between limitations of micro-bolometer technology and limitations of the thermal core when compared to photon detectors.

2.4. Modulation circuit

The circuit developed for heat modulation is based on open source electronics centred on an Arduino Uno microcontroller paired with a

Table 1
Representative size of areas considered and standard deviations.

	Telops FAST IR	FLIR AC655sc	FLIR Lepton 3.5
No. Pixels in 20 mm defective area (Coefficient of Variation)	5000 pixels (0.45%)	17,000 pixels (1.15%)	575 pixels (0.2%)
No. Pixels in 10 mm defective area (Coefficient of Variation)	1700 (0.4%)	4950 pixels (0.95%)	195 pixels (0.165%)
No. Pixels in 5 mm defective area (Coefficient of Variation)	176 (0.35%)	945 (0.85%)	56 pixels (0.175%)
No. Pixels in non-defective area (Coefficient of Variation)	59,630 (1%)	19,000 pixels (2.7%)	8900 pixels (0.5%)

Table 2
IR-Detector Specifications.

Model	MK2 FAST-IR	AC655	Lepton 3.5
Type	Photon Detector	Micro-bolometer	Micro-bolometer
Sensor Type	InSb	VOx	VOx
Cooling Required	Yes	No	No
Manufacturer	Telops	FLIR	FLIR
Max Frame Rate (Full Frame)	100,000 Frame/s	50 Frame/s	8.7 Frame/s
Sensitivity	20 mK	50 mK	50 mK
Time Constant	–	8 ms	8 ms
Array size (x, y) pixels	320, 256	640, 480	160, 120
Relative Cost (Orders of Magnitude)	$	$/10	$/200

MOSFET (Metal Oxide Field Effect Transistor). MOSFETS are commonly used in direct current (DC) switching applications and are of interest as they can be controlled using a low voltage signal to vary its resistance from high (Mega Ohms) to low (<0.1 Ohm). As increasing voltage is applied, the resistance of the MOSFET reduces and current begins to flow. This is a particularly useful for when using microcontrollers and enables control of high-power DC circuitry with comparatively low voltage and current signals. Other attributes are the rapid response of MOSFETs and their low cost.

A schematic of the modulation circuit is shown in Fig. 1. Since the Arduino cannot output an analogue signal, a Digital to Analogue Converter (DAC) is used to produce a sinusoidal signal input into the gate pin of the MOSFET using a 12 bit digital signal from the Arduino and I2C communication protocol. The signal is designed to vary from the MOSFET threshold voltage (1 V) to the peak output voltage of the Arduino (5 V), hence varying the MOSFET resistance from high to low to modulate the flow of current from the 6 V power supply that is also connected to the MOSFET. The output from the MOSFET is a modulated current, which flows through the embedded actuator. As current flows, resistive heating occurs and heat then conducts through the laminate thickness to the observed surface to provide the modulated heating for the LIT. The IR cameras monitor and record an image series of the surface temperature, thereby capturing the thermal response across a field of view.

As the lock-in processing provides notch filtering, a reference signal is required to determine the exact frequency of modulation. Since the MOSFET response is close to instantaneous, the frequency and phase of the voltage signal and the modulated current are assumed identical. Thus, by recording the voltage supplied to the gate pin of the MOSFET, the reference signal is captured. In the case of the photon detector camera the modulation signal is branched and connected to the built in Analogue to Digital Converter (ADC) on the camera. This is convenient as both thermal data and modulation signal are contained in a single output file. Since neither micro-bolometer camera supports recording of external signals, a Picoscope (2000 series) ADC was used to record the reference signal. It would be possible to further reduce costs by using the serial communication of the Arduino for this function, thus avoiding the cost of the ADC. However, due to the exploratory nature of this work, and to avoid undue complication the Picoscope was preferred.

Table 3 summarises the specification of each component used to achieve heating modulation. The exact specification of each component need not be maintained for the construction of a circuit with similar functional performance. Any MOSFET that can be used with a micro-controller, and capable of operating at the current required for heating, will function similarly, and significantly cheaper alternatives are available. Similarly, an Arduino microcontroller is used in this case, to communicate with DAC board. However, a less expensive and more compact alternative is the Atmel ATtiny85 microcontroller, which can simulate I2C and is available for less than 1 USD and is similar in size and weight to a coin (8 × 6 mm) resulting in a total modulation unit mass of less than 100 g.

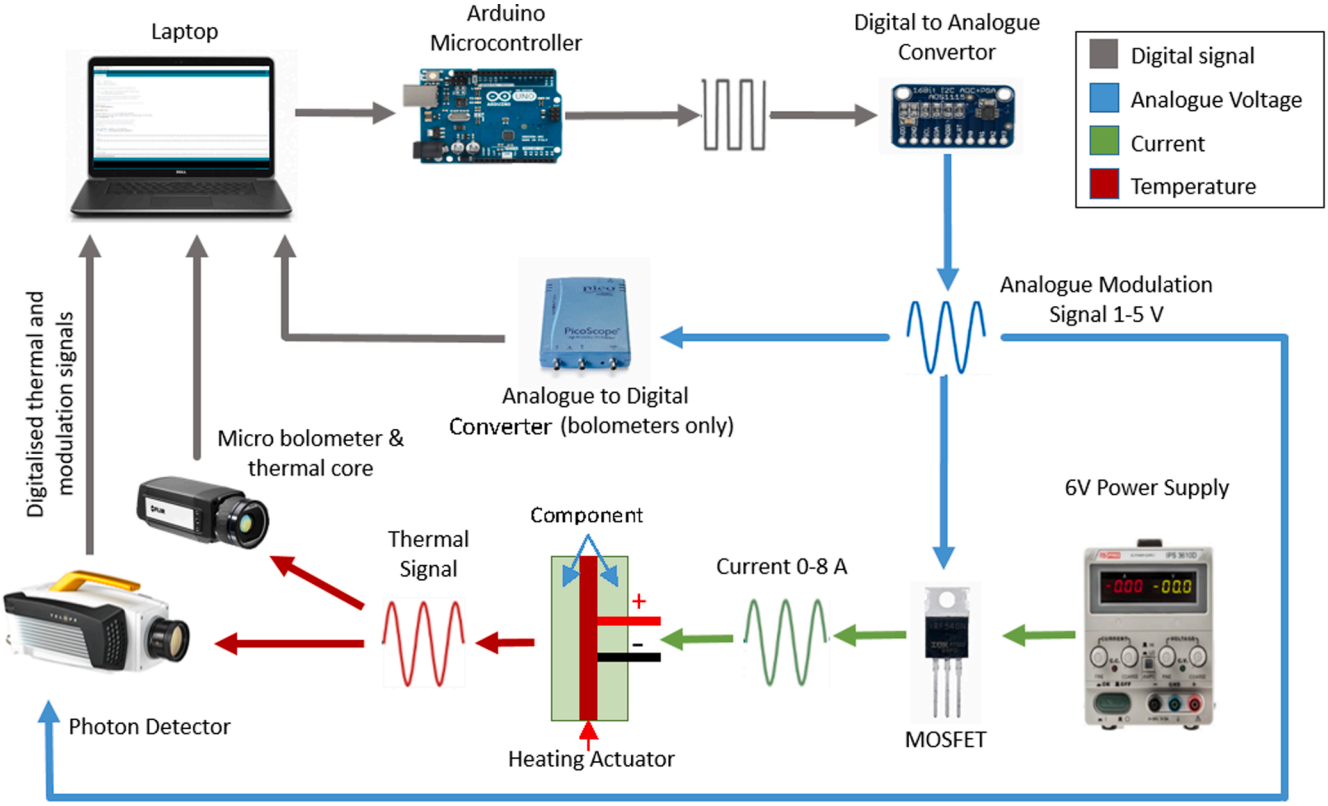

Fig. 1. Schematic of experimental setup.

Table 3
Modulation Circuit Equipment Specification.

Equipment	Description	Specification
Power Supply	Voltage	6 V
	Max Current (observed)	8 A
Heating Device	Supplier	Technical Fibre Products
	Estimated Power	48 W
MOSFET	Manufacturer	International Rectifier
	Model	IRLZ34 NPbF
	Threshold Voltage (GS)	1 V
	Approx. Cost	1 USD
Digital Analogue Converter	Supplier	Adafruit Technologies
	Model	MCP 4725
	Cost	5 USD
Microcontroller	Manufacturer	Arduino
	Model	Uno R3
	Cost	25 USD

2.5. Demonstration specimen

The actuator device used in the study was Carbon Optiveil provided by Technical Fibre Products Global (TFP), which is marketed as an electromagnetic screening material designed to be embedded into composite laminates. While the company do not list the properties of the material publicly, several material properties are presented in [16]. The established use of Optiveil as an embedded material is attractive from an industrial acceptance perspective. The similarity to chopped strand or biaxial carbon fibre was of interest since these materials are often included within laminates to form a hybrid glass/carbon laminate. However, the exact specification of internal actuator implemented could encompass numerous materials and technologies, e.g. metallic materials used for lightning protection in aerospace and wind turbine applications. Indeed the use of an internal actuator within a composite structure was recently demonstrated by Triska *et al.* [21], where a metallic printed circuit board type resistive heating element was placed between the core and face sheet of a sandwich panel. Similar work by De Girogi [22] used shape memory alloy wires embedded within a composite material (as opposed the resistive heater proposed by Triska). In both cases, pulse thermography was used rather than LIT. However, one of the primary motivations for embedding actuators within a component is to improve the probing depth, of the inspection system, and to this end, LIT is better suited for this application. Further, the effect of embedding a printed circuit board heating elements on the structural efficiency of the composite component was not considered. In contrast, the effect on structural performance of the integration of Optiveil used in the demonstrator in the present paper was investigated in [16], which shown no statistically significant structural knockdown. This is of prime importance if embedded actuator system is to be used in industrial applications over traditional externally excited methods. Furthermore, the pre-existing usage of Optiveil in current in-service structures represents a significant advantage in terms of industrial uptake.

For the purposes of demonstrating the technology, a 34 g per square metre carbon veil material was selected for use in this study to ensure the actuator would withstand high currents and generate sufficient heat for use with LIT. Therefore actuator weight compares favourably with the 81 gsm quoted for the heating element described in [21] and presents the opportunity to cover large areas with minimal weight penalty. The heat generated by the chosen material is determined by the current allowed to flow through it. During initial testing of the actuator, prior to embedding in the composite, it was found that 6 V and 8 A generated temperatures of approximately 40 °C. This temperature was determined to be sufficient for the purposes of a thermographic inspection, while still significantly below typical glass transition temperatures of composite resin systems.

Delamination is a particularly common defect in composite materials [23], which has various causes including overloading or impact. Delamination results in an interfacial separation of individual laminae within a cured laminate. To simulate this type of damage, a pre-preg GFRP specimen was manufactured as specified in Table 4, with square shaped Polytetrafluoroethylene (PTFE also known as Teflon) placed between laminate plies. Three sizes (5, 10, 20 mm) of Teflon inserts were used, each positioned at three depths of 0.6, 1.2 and 1.8 mm. To avoid edge effects, the Teflon inserts were placed 20 mm from the edge of the test component. To ensure the thermal response from one Teflon insert did not influence another, all Teflon inserts were separated by 20 mm. The actuator material used was supplied in A4 paper size (210 × 297 mm), hence two actuators were required to provide sufficient spacing between the simulated defects as shown in Fig. 2. The two actuators were placed in the mid plane of a laminate directly under the simulated defects relative to the monitored surface and were separated from the first simulated defect by a single lamina resulting in an effective depth of 1.8 mm from the specimen surface. To simplify the electrical connection, the actuators were mounted to a pre-cured GFRP laminate. Copper tape with an adhesive backing was placed on the pre-cured laminate, on to which the sensors were positioned. The GFRP pre-preg laminate was then laid up on top of the actuators, ensuring a portion of the copper tape remained exposed for electrical connection and the laminate was cured in an autoclave as specified in Table 4. This resulted in an embedded actuator between two laminates, mimicking the encapsulation of a conductive feature in an actual structure. After the laminate had cured, the electrical connections were completed to the actuators by soldering wires to each end.

3. Validation of experimental setup

3.1. Thermal modulation frequency

Previous studies [9] have shown that in LIT inspections the use of higher modulation frequencies allows defects of smaller lateral size to be resolved, yet high frequency thermal waves are easily attenuated. This is of particular concern for inspections of composite materials where thermal waves are highly attenuated by the low thermal diffusivity of laminates. It is possible to estimate the modulation frequency required for an inspection based on the thermal properties of the test component, whereby thicker components typically call for lower modulation frequencies. In many studies e.g. [24], a multitude of frequencies are used in successive inspections, whereby frequencies are tailored for each defect depth, which assume that the defect depth is known *a priori*. However, in real inspections of in-service components, the user does not know the location of defect, or indeed if a defect exists at all, hence, such tailoring is not necessarily practical. Therefore, the range of frequencies of interest were estimated based on the approximate material thermal properties presented in Table 5. The results presented are based on the thermal diffusion length which is equivalent to thermal wave length and hence approximately to the probing depth [9]. The thermal diffusion length μ is given by:

$$\mu = \sqrt{\frac{\alpha}{\pi f}} \tag{6}$$

Table 4
Demonstrator material.

Description	Specification	
Type	Glass Fibre Reinforced Polymer Pre-Preg	
Reinforcement Type	Uniaxial E-Glass	
Number of Plies	8	
Layup	$[0,90,0,90]_s$	
Ply Thickness	0.25 mm	
Laminate Thickness	2 mm	
Pre-Preg System	Manufacturer	PRF Composites
	Type	RP-528
	Cure Temp.	120 °C
	Cure Pressure	3 bar
	Cure Time	2 h

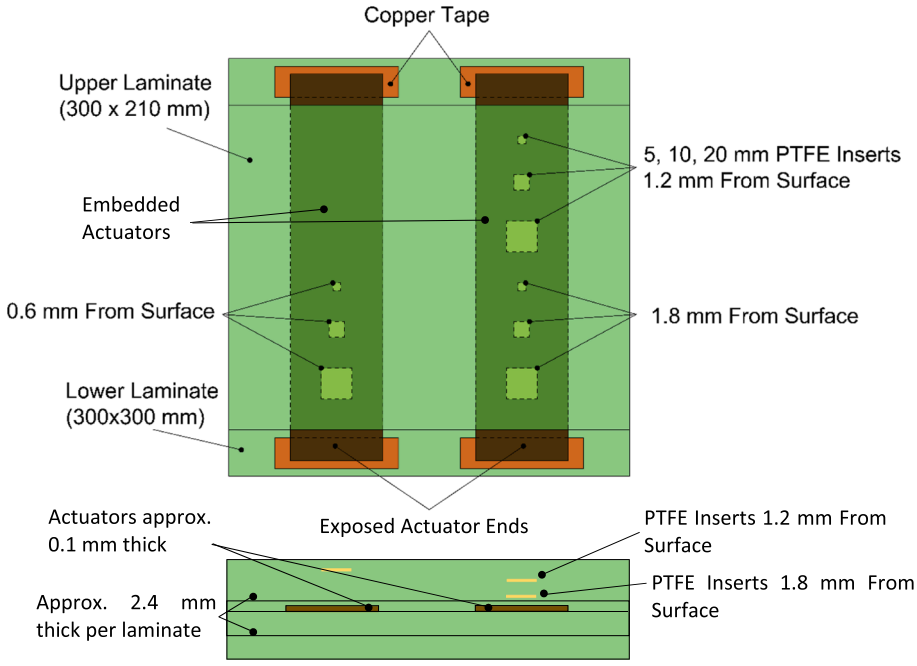

Fig. 2. Schematic of test specimen showing two sensors and three sets of Teflon inserts (not drawn to scale).

Table 5
Thermal properties of E-glass and epoxy resin.

Property	E-Glass Fibres	Epoxy Resin
Thermal Conductivity (W/m.k)	0.5	0.223
Density (kg/m^3)	2600	1200
Specific Heat Capacity (J/Kg°C)	760	1100

where f is the modulation frequency and α is the thermal diffusivity as follows:

$$\alpha = \frac{k}{\rho c_p} \tag{7}$$

where k, ρ, c_p denote thermal conductivity, density and specific heat capacity respectively.

Fig. 3 shows a plot of the theoretical thermal diffusion length against the range of modulation frequencies; beyond 2 Hz the curve is asymptotic. The properties in Eqs. (3) and (4) change with the fibre volume fraction achieved during manufacture of the composite component. To estimate the effect of volume fraction variations, a range of realistic values from 55% to 65% was considered. Fig. 3 shows that the results for each volume fraction are overlaid on each other and hence it can be concluded that fibre volume fraction variations have little effect on the thermal diffusion length for the glass fibre composite material. The results in Fig. 3 were used to optimise the experimental setup and quantify the effect of modulation frequency within bounds of the test configuration used. Hence, a series of experiments were conducted using increasing thermal modulation frequencies from 0.1 to 2 Hz.

To create a baseline, the tests were carried out on the demonstration specimen using the photon detector, with the actuator stimulated at 6 V (0–8 A). A frame rate of 383 frames per second (fps) was used since it is a high prime number relative to the modulation frequency, thus ensuring unique data capture for each modulation cycle. The calculated phase and temperature signal to noise ratio are shown in Fig. 4 and Fig. 5 respectively, for the deepest defects at 1.8 mm depth; it is evident that the signal to noise varies considerably based on the modulation frequency. Both the highest and lowest modulation frequencies have low

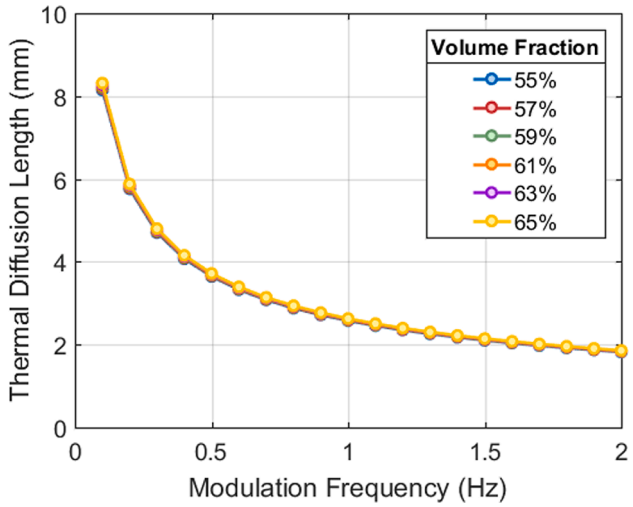

Fig. 3. Theoretical probing depth with varying modulation frequency.

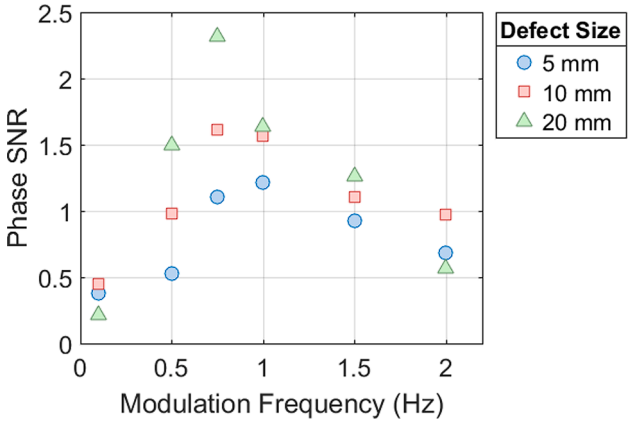

Fig. 4. Effect of modulation frequency on the phase signal to noise ratio (SNR) of defects at 1.8 mm depth.

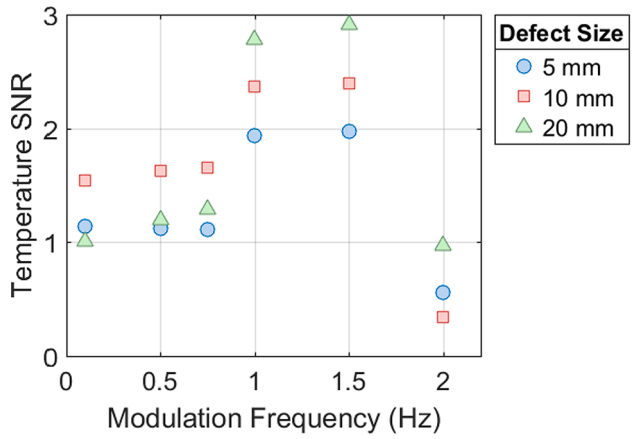

Fig. 5. Effect of modulation frequency selection on amplitude signal to noise ratio (SNR) of defects at 1.8 mm depth.

signal to noise ratio, whilst 1 Hz provides high signal to noise ratio in both phase and temperature amplitude plots dependent on defect size. Therefore, for comparative purposes, and to provide a proof of concept of the proposed inspection methodology, utilising the embedded actuator and compact modulation circuit, it was decided to use a modulation frequency of 1 Hz for all further experiments described in the paper.

3.2. Camera frame rate

The maximum achievable image sampling frequency is referred to here as camera frame rate and reported in units of frames per second (fps) for clarity to make a distinction from the modulation frequency (Hz). Camera frame rate is a key performance attribute that differs between the IR cameras considered in this study. As with any sampling, if the frame rate reduces, the effect of aliasing becomes more pronounced, especially as the Nyquist frequency (i.e. half the camera frame rate [7]) approaches the thermal modulation frequency. Aliasing prevents the lock-in processing from effectively isolating the corresponding thermal response, potentially reducing the achievable signal to noise ratio. Since the photon detector camera is capable of high frame rates, it was used to establish a baseline to understand the extent to which aliasing affects the inspections results. Hence, images were captured at a frame rate of 383 fps, which is significantly higher than the modulation frequencies used in this work and immune from any aliasing as it is a prime number. The temperature and modulation signals were down sampled in Matlab using cubic interpolation to simulate the effect of recording data with lower frame rates. A frequency sweep was carried out in 10 fps increments from 20 fps to 100 fps to capture the onset of aliasing effects. To confirm that useful inspection data could be achieved with all IR cameras used, a further analysis was carried out at the maximum achievable frame rate of the lowest performance micro-bolometer used in this study (8.7 fps).

Data acquired at a modulation frequency of 1 Hz was considered since this showed good signal to noise ratio, as described in the previous section. The effect of frame rates on the signal to noise ratio of the phase of the thermal response is shown in Fig. 6. It can be seen that at frame rates above 40 fps there is no improvement in signal to noise ratio as the frame rate increases. However, for frame rate of less than 20 fps, the signal to noise ratio reduces markedly, suggesting aliasing is affecting the results. Notably, the signal to noise ratio is reduced by approximately two thirds at 8.7 fps, i.e. the frame rate of the thermal core. Nevertheless, the signal to noise ratio is such that it is possible to detect all three defect sizes at 8.7 fps, and therefore from a processing standpoint, the frame rate of the thermal core is not prohibitively low for the purposes of carrying out LIT using the proposed experimental setup.

3.3. Application to micro-bolometers

To make a comparison with traditional inspections, a set of experiments was carried out where the photon detector and thermal core micro-bolometer cameras simultaneously acquired data across approximately the same field of view. This ensured that the experimental conditions, e.g. ambient temperature and modulation frequency were identical across each of the acquired data sets. Due to space restrictions, it was necessary to acquire data with the traditional micro-bolometer separately. Nevertheless the conditions at which the data was acquired were matched as closely as possible to those for the experiments with the photon detector and thermal core, as the laboratory was temperature-controlled and the same modulation frequency settings were used. Each inspection was repeated at all simulated defect depths (0.6, 1.2 and 1.8 mm), whereby the camera positions were kept constant and the test component was translated to achieve a new field of view. For the reasons described above, a thermal modulation frequency of 1 Hz was used all inspections presented in this section. To minimise effects caused by differences in achievable frame rate, the photon detector and traditional micro-bolometer data were subsampled using a cubic interpolation in Matlab to match the maximum achievable frame rate of the thermal core (8.7 fps). For visualisation, all data was normalised by subtracting the mean of the non-defective area. This allowed for common scale across data set for fairer comparison.

Fig. 7 shows the phase signal to noise ratio obtained from the images captured by each of the three cameras viewing the simulated defects at a depth of 1.8 mm. It is clear that all three cameras are able to detect the simulated defects at this depth. The difference in signal to noise ratio between the two micro-bolometers is small, which is of particular

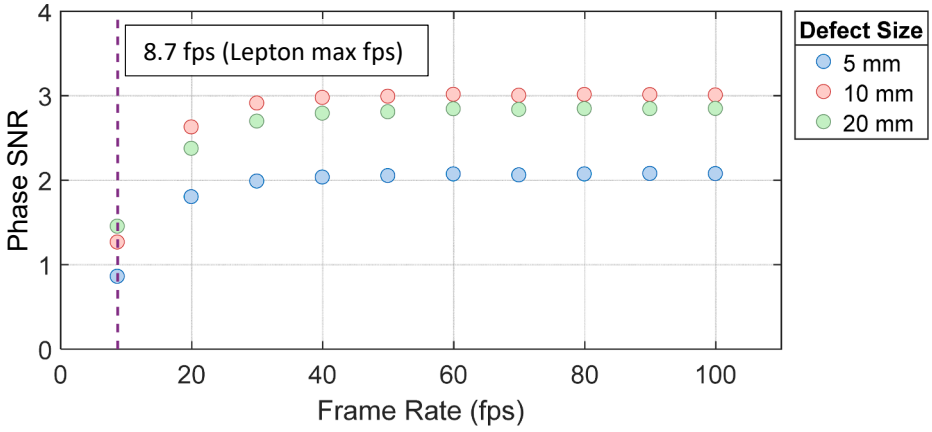

Fig. 6. Effect of frame rate on phase signal to noise ratio (SNR) of defects at 1.8 mm depth using 1 Hz modulation frequency.

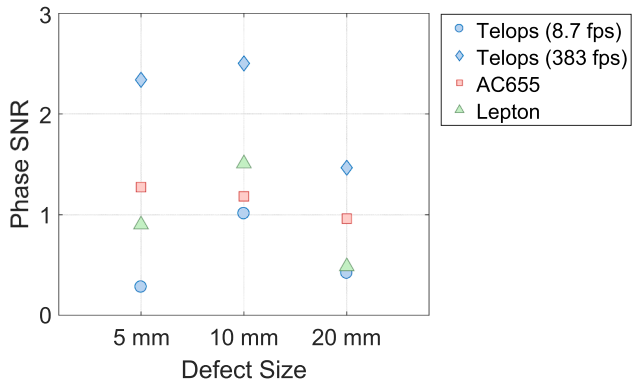

Fig. 7. Comparison of signal to noise ratio (SNR) obtained using each camera 1.8 mm depth.

interest given the significant difference in size and cost of the two cameras. However, it should be noted as discussed previously, that the low frame rate used in this experiment does affect the results obtained and an improvement in signal to noise ratio would be expected for the traditional micro-bolometer and photon detector at higher frame rates. This is illustrated in Fig. 7 where data obtained at 383 fps with the photon detector is presented alongside data subsampled to 8.7 fps, indicating that the ability of the photon detector to record temporally rich data yields significantly higher signal to noise ratio than the thermal core micro bolometer.

Fig. 8 provides additional insights, where the full-field phase images obtained from all three cameras is compared. In Fig. 8 (a) the image from the photon detector shows all three defect sizes (5, 10 and 20 mm) are clearly identified and well characterised. Similarly, Fig. 8 (b) and (c) show the data obtained from both micro-bolometers identified the defects. In comparing the data of the smallest defect in all three, the effect of sensor size is apparent, where the approximate resolution of 3.5, 7.3 and 1.2 pixels/mm for the photon detector, micro-bolometer and thermal core cameras respectively results in the smallest defect being best characterised with the highest resolution detector. Furthermore, the edges of the defects and overall sharpness of detail is best captured in Fig. 8(b) where the camera has a superior spatial resolution afforded by greater number of pixels/mm. The inverse of this is evident for the thermal core camera data in Fig. 8 (c) where a significantly lower spatial resolution is available. Fig. 8 (d) is included to visualise the results obtained when acquiring data with the photon detector at 383 fps, showing a strong contrast between defective and non-defective areas. Fig. 8 (c) shows some distortion of the defect shape which is most noticeable in the 20 mm defect caused by the wide-angle lens fitted to the thermal core camera. This effect is also amplified by the position of the camera at an oblique angle to accommodate the two cameras used simultaneously in this test and could be minimised by positioning the camera perpendicular to the inspection surface.

Fig. 9 shows the signal to noise ratio obtained from the simulated defects at the shallower depth of 1.2 mm for the three cameras, with the photon detector outperforming the micro-bolometers. Comparing the data qualitatively, all three defects are clearly identified in the phase images shown in Fig. 10. The difference in response based on defect size follows the same trend for both micro-bolometer cameras, with the

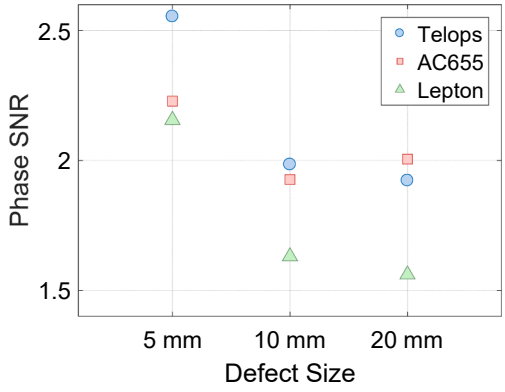

Fig. 9. Comparison of signal to noise ratio (SNR) obtained using each camera, 1.2 mm depth 1 Hz modulation frequency.

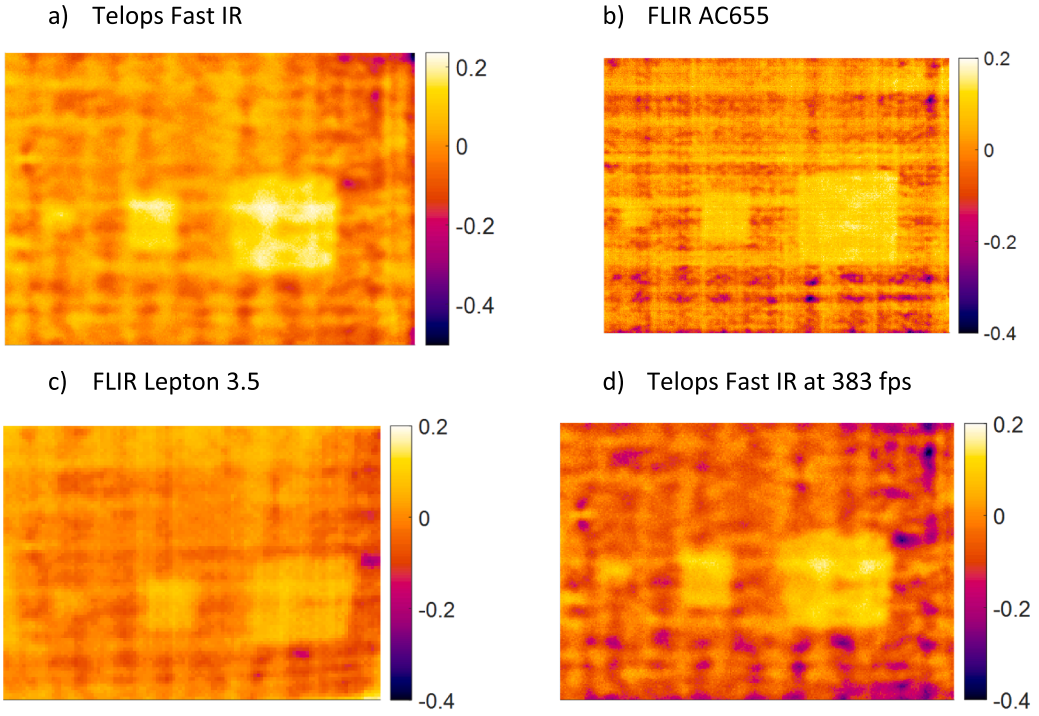

Fig. 8. Visual comparison of phase data of simulated defects at 1.8 mm at 1 Hz modulation frequency normalised by subtracting mean of non-defective area.

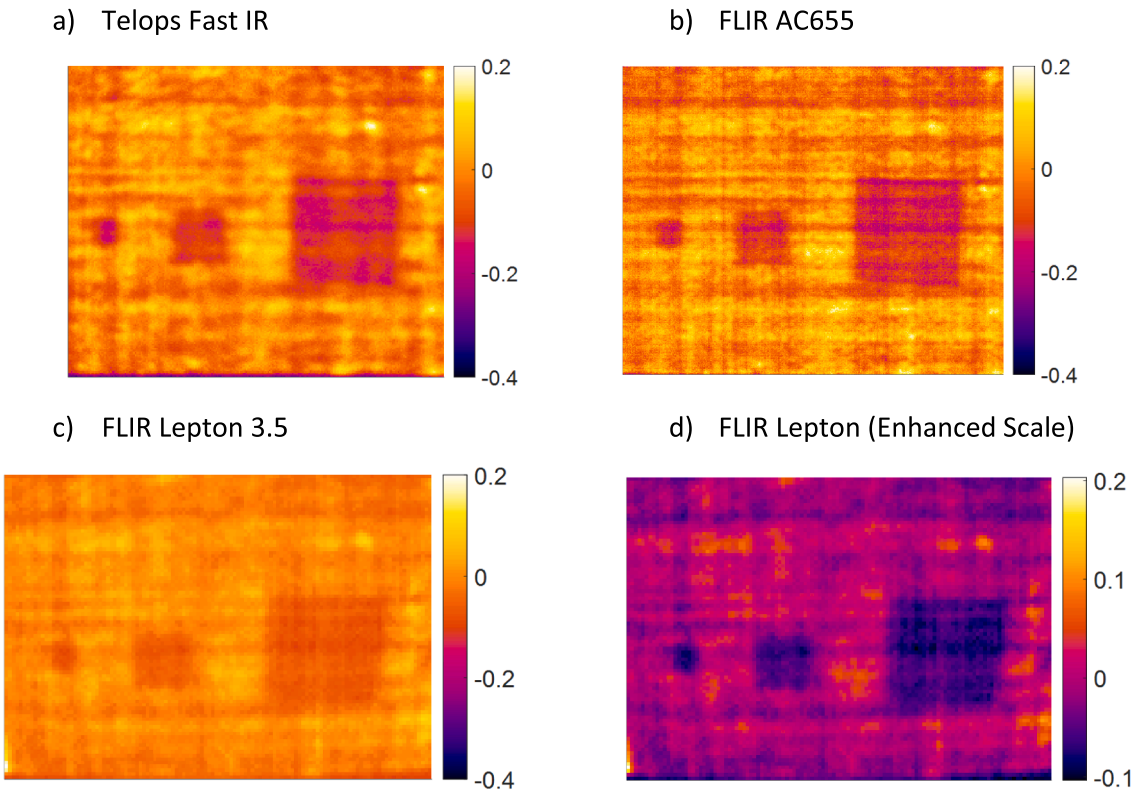

Fig. 10. Visual comparison of phase data of simulated defects at 1.2 mm at 1 Hz modulation frequency normalised by subtracting the mean of the non-defective area.

thermal core resulting in a marginally lower signal to noise ratio than the traditional micro-bolometer. It is important to note that the signal to noise ratio for all cameras and defects sizes for the 1.2 mm deep defect is similar to that obtained at for the 1.8 mm deep defect (see Fig. 7). This is to be expected when external excitation is applied where typically the shallowest defects are closest to both the IR camera and the heat source and hence provide a greater signal to noise ratio. In the current arrangement, the deepest defects are located closest to the heat source and therefore experience the highest temperatures, and reduction in signal to noise ratio with increasing depth is less pronounced than may typically be expected. One negative implication of strong thermal contrast at deep locations is that lateral (in plane) thermal gradients will also be strongest for the deepest defect, which encourages lateral diffusion and results in blurring of defect edges in the visualised data. Based on the visualisations included in this work, the laminates do not appear to be sufficiently thick for lateral diffusion to become apparent, but this may influence results obtained from thicker laminates.

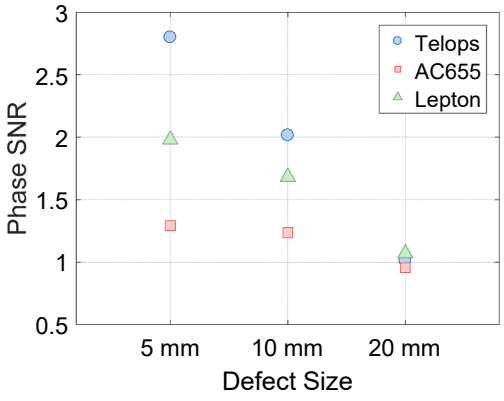

Fig. 11. Comparison of signal to noise ratio (SNR) obtained using each camera, 0.6 mm depth 1 Hz modulation frequency.

Fig. 11 shows that similar trends are observed in the data obtained from the simulated defects at the shallowest depth 0.6 mm. While the signal to noise ratio obtained from the photon detector is higher than the signal to noise ratio obtained using the thermal core as shown in Fig. 12 (a) and (c), where the same scale is used. However, a small adjustment to the scale Fig. 12 shows the thermal core performs well for defect characterisation when compared to the photon detector. The edges of the square shaped defect appear more clearly defined in Fig. 9 (c/d) than (a). However, it should be noted that the frame rate has been intentionally reduced to match the thermal core and higher signal to noise ratio may be possible at the higher frames available with the traditional micro-bolometer and the photon detector. In addition, further optimisation of the modulation frequency could be implemented to improve the results.

4. Conclusions

The work has met the aims stated in the introduction by demonstrating:

1. Existing conductive internal features can be used as a heating actuator, as demonstrated with Optiveil inclusions, showing that sufficient heat can be generated to reveal defects in glass-fibre epoxy composite laminates at 1.8 mm depth.
2. Low-cost open source electronics and an inexpensive light weight miniature camera can be combined to form an effective inspection system eliminating the need for bulky and expensive modulation units.
3. The low sensitivity of thermal core cameras can be overcome using lock-in processing to provide useful thermogaphic inspection data successfully identifying all simulated defects at all depths tested.

In applications where absolute performance outweighs equipment

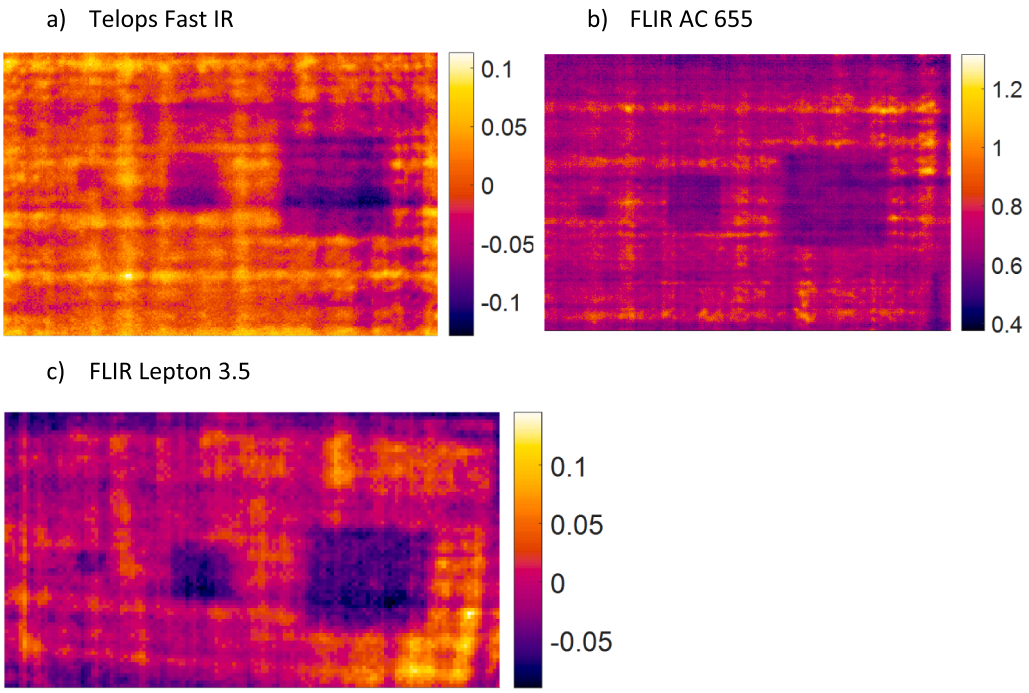

Fig. 12. Visual comparison of phase data of simulated defects at 0.6 mm at 1 Hz modulation frequency normalised by subtracting mean of the non-defective area.

size and cost considerations, photon detectors remain a superior choice where low noise and high sensor sensitivity yield high phase signal to noise ratio. In addition, their high spatial and temporal resolution provide advantages in both processing flexibility and data visualisation. When the photon detector was used at low frame rates to match the capability of the thermal core, the photon detector provided comparatively high signal to noise ratio and outperformed the micro-bolometers in some cases. However, as photon detectors generally require cooling, the cameras are larger and heavier than the uncooled micro-bolometer cameras, and there are many applications where the high equipment cost, size and mass prohibit the use of photon detectors. The results obtained from both micro-bolometers demonstrated that they performed adequately, with all simulated defects visible and well characterised in the phase data obtained at all depths considered. In particular, the traditional micro-bolometer with its high spatial resolution identified the defect edges accurately and hence the overall shape. Most promisingly, the relatively cheap printed circuit board mounted thermal core type micro-bolometer provided good signal to noise ratio results and was able to clearly identify the deepest defects. The small size and low weight of the thermal core camera could allow for their permanent placement as a monitoring device on, or within, an in-service structure. The embedded nature of the proposed actuator is perfectly suited to such applications, providing a non-invasive and lightweight, highly controllable source of heat. This combined with the thermal core micro bolometers, for the first time demonstrates the potential of permanently deploying miniature thermal core infra-red cameras for the purpose of cost-effective full-field structural health monitoring without significant weight penalty.

In summary, the work presented in the paper provides an important proof of concept of both internal thermal excitation and low cost micro-bolometers for LIT inspections. The combination of increased probing depth and significantly reduced costs and weight will considerably broaden access to thermography in new industrial and academic applications. Furthermore, while the low cost and compact modulation circuit was conceived for the purpose of demonstrating the internal actuation methodology, it can be used to control any heating actuator which uses direct current, e.g. halogen lamps used in traditional LIT inspections.

CRediT authorship contribution statement

G. Ólafsson: Writing - original draft, Conceptualization, Formal analysis, Visualization. **R.C. Tighe:** Conceptualization, Supervision, Writing - review & editing. **S.W. Boyd:** Conceptualization, Supervision, Writing - review & editing. **J.M. Dulieu-Barton:** Conceptualization, Supervision, Writing - review & editing, Funding acquisition.

Declaration of Competing Interest

The authors declare that they have no known competing financial interests or personal relationships that could have appeared to influence the work reported in this paper.

Acknowledgements

The authors would like to thank the Engineering and Physical Sciences Research Council (EPSRC) and BAE Systems Naval Ships for funding the work with an industrial PhD CASE studentship. The work described in the paper was conducted in the Testing and Structures Research Laboratory (TSRL) at the University of Southampton and the authors are grateful for the support received from Dr Andy Robinson, the TSRL Experimental Officer. The authors thank Mr. Michael Caton of TFP for supplying the material to develop the embedded actuator. The authors also appreciate the guidance and support of the student electronics workshop at the University of Southampton during the development of the modulation circuitry. The authors also thank Dr Cedric Devivier for contributing to the lock-in processing used in this study.

References

[1] W.J. Cantwell, J. Morton, The significance of damage and defects and their detection in composite materials: A review, J. Strain Anal. Eng. Des. 27 (1) (1992) 29–42, https://doi.org/10.1243/03093247V271029.
[2] A. Katunin, K. Dragan, M. Dziendzikowski, Damage identification in aircraft composite structures: A case study using various non-destructive testing techniques, Compos. Struct. 127 (2015) 1–9, https://doi.org/10.1016/j.compstruct.2015.02.080.

[3] V.P. Vavilov, D.D. Burleigh, Review of pulsed thermal NDT: Physical principles, theory and data processing, NDT E Int. 73 (2015) 28–52, https://doi.org/10.1016/j.ndteint.2015.03.003.
[4] G. Busse, D. Wu, W. Karpen, Thermal wave imaging with phase sensitive modulated thermography, J. Appl. Phys. 71 (8) (1992) 3962–3965, https://doi.org/10.1063/1.351366.
[5] D. Wu, G. Busse, Lock-in thermography for nondestructive evaluation of materials, Rev. Gen. Therm. 37 (8) (1998) 693–703, https://doi.org/10.1016/S0035-3159(98)80047-0.
[6] J.C. Krapez, G. Gardette, D. Balageas, Lock-in IR thermography - Advantages and problems of some approaches, in: International Workshop on Advanced Infrared Technologies and Applications, 1995, no. July, [Online]. Available: http://md1.csa.com/partners/viewrecord.php?requester=gs&collection=TRD&recid=A9632095AH.
[7] G. Ólafsson, R.C. Tighe, J.M. Dulieu-Barton, Improving the probing depth of thermographic inspections of polymer composite materials, Meas. Sci. Technol. 30 (2) (Feb. 2019), 025601, https://doi.org/10.1088/1361-6501/aaed15.
[8] T. Dursun, C. Soutis, Recent developments in advanced aircraft aluminium alloys, Mater. Des. 56 (2014) 862–871, https://doi.org/10.1016/j.matdes.2013.12.002.
[9] G. Busse, Optoacoustic phase angle measurement for probing a metal, Appl. Phys. Lett. 35 (10) (1979) 759–760, https://doi.org/10.1063/1.90960.
[10] K. Chatterjee, S. Tuli, S.G. Pickering, D.P. Almond, A comparison of the pulsed, lock-in and frequency modulated thermography nondestructive evaluation techniques, NDT E Int. 44 (7) (2011) 655–667, https://doi.org/10.1016/j.ndteint.2011.06.008.
[11] G.M. Carlomagno, C. Meola, Comparison between thermographic techniques for frescoes NDT, NDT E Int. 35 (8) (2002) 559–565, https://doi.org/10.1016/S0963-8695(02)00029-4.
[12] D. Palumbo, R. Tamborrino, U. Galietti, P. Aversa, A. Tatì, V.A.M. Luprano, Ultrasonic analysis and lock-in thermography for debonding evaluation of composite adhesive joints, NDT E Int. 78 (2016) 1–9, https://doi.org/10.1016/j.ndteint.2015.09.001.
[13] J.E. Thatcher, D.A. Crump, C. Devivier, P.B.S. Bailey, J.M. Dulieu-Barton, Low cost infrared thermography for automated crack monitoring in fatigue testing, 2019, p. 105914, Opt. Lasers Eng. 126 (May) (2020), https://doi.org/10.1016/j.optlaseng.2019.105914.
[14] S.G. Pickering, D.P. Almond, An evaluation of the performance of an uncooled microbolometer array infrared camera for transient thermography NDE, NDT E Int. 22 (2–3) (2007) 63–70, https://doi.org/10.1080/10589750701446484.
[15] R. Bayareh, A. Vera, L. Leija, J. Gutierrez-Martinez, "Programming of a system for the acquisition of images and thermographic data for the diabetic foot analysis, in: *2017 14th Int. Conf. Electr. Eng. Comput. Sci. Autom. Control. CCE 2017*, 2017, pp. 2–8. http://dx.doi.10.1109/ICEEE.2017.8108866.
[16] G. Ólafsson, R.C. Tighe, S.W. Boyd, J.M. Dulieu-Barton, Development of an Integrated Sacrificial Sensor for Damage Detection and Monitoring in Composite Materials and Adhesively Bonded Joints, Struct. Heal. Monit. 20 (6) (2021) 3406–3423, https://doi.org/10.1177/1475921721989041.
[17] R. Shrestha, Y. Chung, W. Kim, Wavelet transform applied to lock-in thermographic data for detection of inclusions in composite structures: Simulation and experimental studies, Infrared Phys. Technol. 96 (July 2017) (2019) 98–112, https://doi.org/10.1016/j.infrared.2018.11.008.
[18] N. Tabatabaei, A. Mandelis, B.T. Amaechi, Thermophotonic radar imaging: An emissivity-normalized modality with advantages over phase lock-in thermography, Appl. Phys. Lett. 98 (16) (2011) 1–4, https://doi.org/10.1063/1.3582243.
[19] P.A. Temple, An introduction to phase-sensitive amplifiers: An inexpensive student instrument, Am. J. Phys. 43 (9) (1975) 801–807, https://doi.org/10.1119/1.9690.
[20] V. Vavilov, Evaluating the efficiency of data processing algorithms in transient thermal NDT, vol. April 2004, 2004, pp. 336. http://dx.doi.10.1117/12.537604.
[21] V. Třískа, T. Chlebeček, J. Hnidka, K. Maňas, Testing of the heating element integrated into the honeycomb sandwich structure for active thermography inspection, J. Sandw. Struct. Mater. (2020), https://doi.org/10.1177/1099636220927888.
[22] M. De Giorgi, R. Nobile, A. Saponaro, Numerical and experimental validation of SMArt thermography for the inspection of wind blade composite laminate, SN Appl. Sci. 2 (10) (2020) 1–19, https://doi.org/10.1007/s42452-020-03428-0.
[23] R.D. Adams, P. Cawley, A review of defect types and nondestructive testing techniques for composites and bonded joints, NDT Int. 21 (4) (Aug. 1988) 208–222, https://doi.org/10.1016/0308-9126(88)90333-1.
[24] S. Ranjit, K. Kang, W. Kim, Investigation of lock-in infrared thermography for evaluation of subsurface defects size and depth, Int. J. Precis. Eng. Manuf. 16 (11) (2015) 2255–2264, https://doi.org/10.1007/s12541-015-0290-z.